Images of the Vortex Chain State in Untwinned $YBa_2Cu_3O_{7-\delta}$ Crystals

P. L. Gammel and D. J. Bishop

AT&T Bell Laboratories, Murray Hill, New Jersey 07974

J. P. Rice and D. M. Ginsberg

Department of Physics, University of Illinois, Urbana, Illinois 61801
(Received 18 March 1992)

A vortex lattice consisting of a pinstripe pattern of vortex chains has been observed in untwinned $YBa_2Cu_3O_{7-\delta}$ crystals. This state is present when the field is tilted away from the $\hat{c}$ axis, and is oriented with the chains confined to the plane defined by $\mathbf{B}$ and $\hat{c}$. The chains arise from the attractive part of the vortex-vortex interaction in this geometry as described within the anisotropic London equations. For $B > \Phi_0/2\pi\lambda^2$ the chains merge into an oriented vortex lattice. From the fitted value of $\tilde{\lambda}$, we can conclude that the microscopic irreversibility temperature is $T/T_c \sim 0.92$ for $B \sim 20$ G.

It is essential to understand the equilibrium structure of the flux-line lattice in an anisotropic superconductor. This structure is reflected in NMR, neutron scattering, and μSR line shapes. Calculation of elastic constants, and the associated problems of pinning and plasticity, require as input the correct equilibrium vortex configuration.

For fields applied parallel to the anisotropy axis, corresponding to the c axis in the high-T_c superconductors, studies [1] in $YBa_2Cu_3O_{7-\delta}$ (YBCO), $Bi_{2.1}Sr_{1.9}Ca_{0.9}Cu_2O_{8+\delta}$ (BSCCO), and $NbSe_2$ have all observed a weakly distorted Abrikosov flux lattice. The weak distortions [1,2] in YBCO and BSCCO are understood as arising from a small in-plane effective mass anisotropy. Direct images which probe the large anisotropy direction have been more elusive. Dolan et al. [2] were able to observe flux structures and oval vortices on the a-c face in a few YBCO crystals. These observations were in rough agreement with estimates of the more severe distortion arising from effective mass anisotropy in that case, but clearly also depicted dynamical and pinning effects. The flux lines in BSCCO in tilted fields [3] form a very unusual chain structure which has yet to be understood.

Here, we report on the structure of YBCO flux lattices in tilted fields, imaged with high-resolution Bitter patterns. The essence of our result is apparent in the dramatic photograph of Fig. 1. The vortex lattice is transformed into a pinstripe array of vortex chains, oriented to lie in the plane defined by $\mathbf{B}$ and $\hat{c}$. Such a structure had been predicted [4] in the low-field limit from the anisotropic London equations. Our results, as described in detail below, are in quantitative agreement with these calculations. As the applied field is increased, we find that the chains merge smoothly into an isotropic vortex lattice, still oriented in the same direction. This crossover field agrees with recent numerical simulations [5].

The samples [6] used in this experiment were irregular pieces of single-crystal YBCO with untwinned regions of at least 100 μm square. The pieces were flat platelets roughly 0.5 mm×0.5 mm in the a-b plane. The

thicknesses varied considerably—ranging from 5 to 40 μm. Decoration studies with the field applied parallel to the c axis show an order-disorder transition [7] in the flux lattice at $B \sim 10$ G in the untwinned regions. This suggests for fields of this magnitude or larger, the flux-lattice structure is not strongly influenced by the microscopic pinning. Naturally, the strong pinning at the twin boundaries substantially modifies the local vortex positions [8]. This distortion of the vortex lattice, however, only extends about 4–5 lattice constants from the twin plane for the fields of 10–100 G studied here. In this paper we will describe the structure far removed from this or any other obvious defect.

The flux lines were imaged using high-resolution Bitter patterns [9]. Samples with a surface clean and free from any obvious surface morphology were first examined under polarized light. The polarized light image was used to identify the position and direction of the twin planes. The samples were mounted with the c axis at a fixed an-
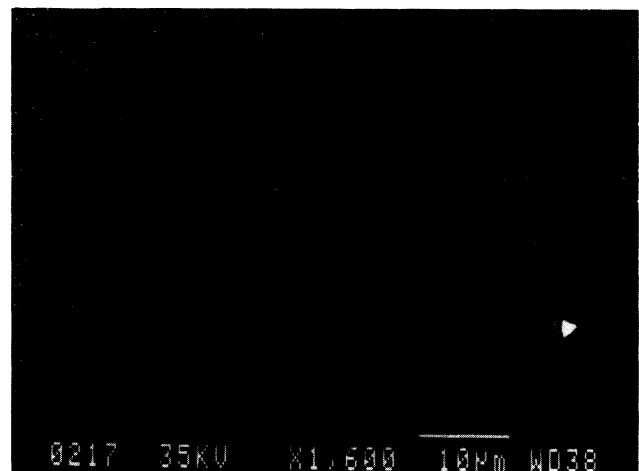

FIG. 1. SEM micrograph of the vortex chains with a field of 24.8 G applied at 70° from the $\hat{c}$ axis of the crystal. The chains lie in the plane defined by $\mathbf{B}$ and $\hat{c}$. The resultant image is independent of the direction of the $\hat{a}$ axis, which in this picture runs approximately 45° from the chains.

gle with respect to the applied magnetic field. Generally, the $\hat{a}$ or $\hat{b}$ axis was aligned so that a clean and straight facet was perpendicular to the plane formed by **B** and $\hat{c}$ in order to look for additional vortices on this face. Decorations with the in-plane crystal lattice in other directions show the chain structure described here to be independent of crystallographic orientation. The present work involved 25 separate decorations using ~30 crystallites. The decorations were successful about 80% of the time, allowing us to obtain systematic results.

For a magnetic field of 24.8 G applied at an angle of 70° from the c axis, the resulting chain structure is shown in the scanning electron microscopy (SEM) micrograph of Fig. 1. As stated above, the chains lie in the plane defined by **B** and $\hat{c}$. In early calculations [10], this was found to be the preferred orientation for a distorted vortex lattice in the anisotropic London limit. Defects in the chain structure shown in Fig. 1 are clearly seen, mostly in the form of edge dislocations. The first analysis of this structure involves the average vortex density. In Fig. 2, this density, normalized to the applied field, is shown versus the angle between **B** and $\hat{c}$. Within measurement error, the normal component of the applied field induces the observed vortex structure.

Our attempts to see vortices on the face of the crystal perpendicular to this one always failed. In general, it appears that demagnetizing effects allow for substantial flux expulsion near the edge of the crystals at high tilt angles. Hence, we will only discuss the features observed on the a-b face.

To continue the quantitative analysis, we define D to be the vortex spacing along the chains, and C the spacing between chains, as sketched in the inset of Fig. 2. Note that in the limit of an isotropic vortex lattice this reduces

to $C = D\sqrt{3}/2$ with $\phi_0/B = CD$. This definition is the same as was used to describe the vortex chains observed [3] previously in BSCCO. We focus first on the intrachain spacing D, shown versus the normal field component for several fixed angles in Fig. 3.

For an isotropic vortex lattice, $D = 4.89B^{-1/2}$ μm with B in gauss. For both data sets, the observations fall below this value, as is implicit in the notion of vortex chains. As the angle is increased, the field dependence of D decreases. Solution of the anisotropic London equations [4] in the limit $H \rightarrow H_{c1}$ reveals an attractive well in the in the vortex-vortex interaction in the direction along the chains. The vortices in fields just above H_{c1} will sit in these wells—thereby forming the chains. The spacing between chains is set by the requirement that the average vortex density be correct. For this experiment, this leads to a constant D and $C \sim 1/B$. Although the initial calculations only examined the potential due to a single vortex, it is possible to include the interactions along the chain direction, ignoring interchain interactions. While this is valid just above H_{c1}, it clearly needs to be modified when the intrachain and interchain spacings are comparable. Roughly, one understands the attractive well as arising from the tendency of the current paths to stay in the a-b plane, coupled with the observation that two dipoles attract when parallel and oriented along the line joining them.

More detailed comparison can be pursued through an examination of the angle dependence of D. We have tak-
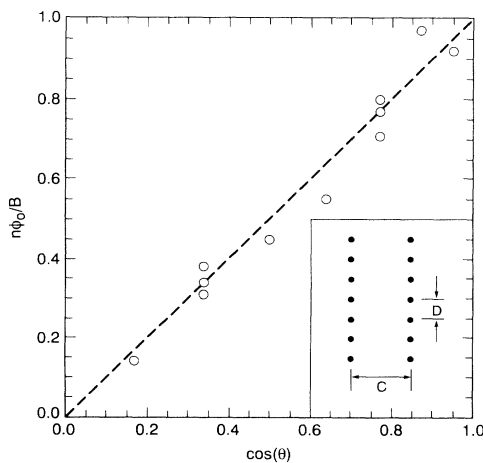

FIG. 2. The measured vortex density on the crystal surface normalized to the applied field is plotted against the angle of the applied field with respect to the $\hat{c}$ axis. Hence, the normal component of the applied field is responsible for the observed vortex density. Inset: Geometry of the vortex chains.
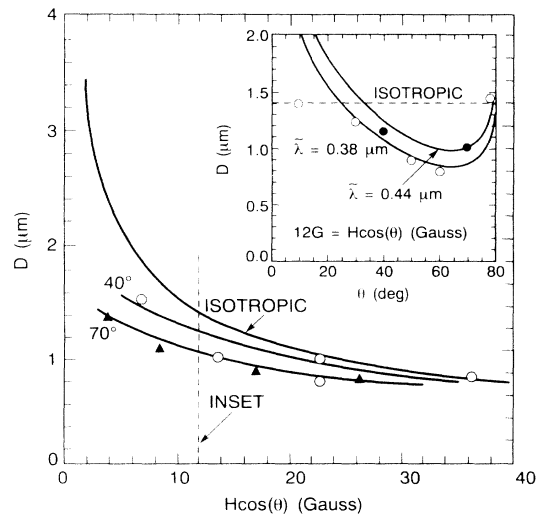

FIG. 3. The intrachain vortex spacing vs normal field component at fixed angles of 40° and 70°. The open circles are for the data taken at 40° and the closed triangles are for the 70° data. The lines through the data are guides to the eye. Also shown is the limit of an isotropic vortex lattice. Inset: The angle dependence is shown for a normal field component of 12 G. The open and closed symbols are explained in the text. Two fits are shown with $\tilde{\lambda} = 0.44$ and 0.38 μm. Also shown by the dashed line is the limit for an isotropic vortex lattice.

en data at a fixed normal field component of 12 G, as shown by the open circles in the inset to Fig. 3. The two solid points are interpolations from the field dependence in the main part of the figure. This is the lowest field at which accurate and systematic data on the chains can be obtained.

The dashed line is what would be expected for an isotropic vortex lattice. The two solid lines are the low-field calculations for D using $\tilde{\lambda}=0.44$ μm for the upper curve and $\tilde{\lambda}=0.38$ μm for the lower. In this expression, the average penetration depth $\tilde{\lambda}$ is defined as $\tilde{\lambda}=(\lambda_a\lambda_b\lambda_c)^{1/3}$. The square root of the effective mass ratio γ has been assumed to be 5. The solid lines are reliable fits only when they fall below the dashed line. When the calculation for D exceeds the isotropic limit at low angles, the neglected interchain effects will be a dominant contribution to the interactions. A natural extension of the low-field theory is a simple graphical interpolation using the inset to Fig. 3. The actual value of D will likely reflect the smaller of the values presented by the solid and dashed lines and be a smooth interpolation between them. Of course, a full calculation may revise the estimate of $\tilde{\lambda}$.

At zero temperature, $\tilde{\lambda}=0.28$ μm from values given in the literature [11]. In order to explain our data, it is then necessary to assume that the pattern is frozen in at a temperature close to T_c where the penetration depth is considerably larger. Using the two-fluid model [12] for the temperature dependence of the penetration depth, this implies $0.83 < T/T_c < 0.88$, which is plausible, but still well below the irreversibility temperature measured via bulk magnetization.

The possibility that the microscopic irreversibility temperature, where the topology of the vortex lattice becomes fixed, lies below the bulk irreversibility line has been suggested previously [1]. There remain, however, several caveats. Increasing γ from 5 to the more generally accepted [13] values of 7-8 would increase the fitted $\tilde{\lambda}$ by $\sim 50\%$. Such an increase would also increase the curvature of D vs θ at high angles, which would seem to give better agreement with these results. Even so, this implies $T/T_c \sim 0.95$, well below the expected irreversibility point $T/T_c \sim 0.998$ for this field. Of course, so close to T_c, the two-fluid form gives estimates for T/T_c which are lower than the extreme anomalous limit. The exact form of $\lambda(T)$ close to T_c for the oxide superconductors is difficult to determine [14], and will not be pursued further here. Finally, recent torque measurements [13] on untwinned crystals have shown a much larger regime of reversible behavior, consistent with the results presented here.

Within this model, the increase in D at low fields could be explained by the extreme sensitivity of $\tilde{\lambda}$ on the equilibrium temperature in this range. One would expect the irreversibility temperature to fall closer to T_c at lower fields, in agreement with the measured D which requires an increased $\tilde{\lambda}$ at low fields. One should also note that at extremely low fields, the chains are replaced by an amor-

phous array of vortices. In the 70° case, at 4 G, the sample had a mixture of chains and amorphous vortices. For 40° and 4 G, only an amorphous vortex array was present. These fields are below the order-disorder transition mentioned above, so pinning is probably playing a dominant role. The shallow minimum in the vortex-vortex interaction similarly makes dynamical considerations [5] likely to influence the pattern at very low fields.

As the magnitude of the applied field is increased the chains merge smoothly and finally form an oriented, isotropic vortex lattice. Numerical simulations suggest that this crossover should occur at a field $B\sim(\phi_0/2\pi\tilde{\lambda}^2)$. With the estimates for the effective $\tilde{\lambda}$ found above, the crossover field should be near 20 G, in qualitative agreement with our data. This further strengthens the estimates for the equilibrium value of T/T_c given above.

The data for the interchain spacing is shown in Fig. 4. Basically, this should be given by the intrachain spacing and the average density requirement. Combining the two data sets, one can see that the ratio C/D increases at low fields, and makes the chain structure even more prominent. In the simple chain approximation $C\sim\phi_0/\tilde{\lambda}B$, crossing over to $C=4.23/\sqrt{B}$ μm in the isotropic limit. The crossover field should be the same as discussed for D and the data are consistent with this.

It is important to understand that this structure is substantially different, and presumably arises from different physics, from the chainlike structure previously reported [3] in BSCCO. This is clear from the experimental data. Unlike BSCCO, the structure described here does not scale simply with the field. In BSCCO the morphology was field independent, but with the distance scale set by the field. As shown above, in YBCO the pattern changes
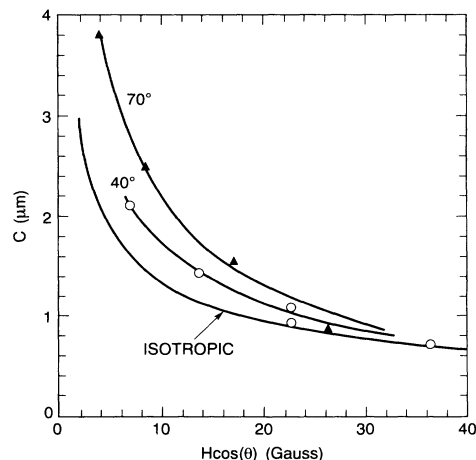

FIG. 4. The interchain spacing vs normal field component for different fixed angles. The solid lines are guides to the eye; also shown is the limit of an isotropic vortex lattice. With our definitions $C=D\sqrt{3}/2$ in the isotropic limit. As in Fig. 3, the open circles correspond to the 40° case, and the closed triangles to 70°.

with field. This is a consequence of the fixed length in the problem—the attractive well—which depends on λ and θ, but not on the applied field. In YBCO, the flux-line lattice has chains only—there is no superlattice modulation as in BSCCO.

It appears that YBCO is the simple case, fully explicable within the anisotropic London equations. This was not possible in BSCCO. We now believe [15] that the structure in BSCCO actually represents two sublattices of vortices running essentially orthogonal to one another. One sublattice is the Abrikosov lattice which dominates the picture. The second sublattice of Josephson vortices causes the superlattice modulation as the vortices attract each other when orthogonal. Hence the "chains" in that case are actually an image of vortices running parallel to the a-b plane. That two such sublattices should appear is implicit in the flux-line free energy calculated [16] by Sudbo and Brandt, which shows two pronounced minima as a function of angle for certain applied fields.

In summary, direct images have shown that the low-field flux lattice in untwinned YBCO in tilted fields is composed of a pinstripe array of vortex chains. These chains lie in the plane defined by $\mathbf{B}$ and $\hat{\mathbf{c}}$, and are related to the attractive part of the vortex-vortex interaction in this direction. Roughly, the vortex spacing in the chains is independent of field at low fields. At high fields, the structure smoothly maps onto an oriented vortex lattice. The detailed field and angle dependence can be understood quantitatively from the anisotropic London equations, if one assumes $\tilde{\lambda} \sim 0.4$ μm. This value of the penetration depth can be accounted for if the structure we observe is a frozen-in vestige from the microscopic irreversibility temperature $T/T_c \sim 0.92$.

We would like to thank D. Huse, A. Sudbo, V. Kogan, L. Daemon, and L. Campbell for helpful discussions. Part of this work has been supported by the National Science Foundation through Grant No. DMR-90-17371.

---

[1] This subject has been reviewed by D. J. Bishop et al., Science 255, 165 (1992); also P. L. Gammel, in Phenomenology and Applications of High Temperature Superconductors, edited by M. Inui and K. Bedell (Addison-Wesley, New York, 1992).

[2] G. J. Dolan et al., Phys. Rev. Lett. 62, 2184 (1989).

[3] C. A. Bolle et al., Phys. Rev. Lett. 66, 112 (1991).

[4] B. I. Ivlev and N. B. Kopnin, Phys. Rev. B 44, 2747 (1991); B. I. Ivlev et al., Phys. Rev. B 43, 2896 (1991); V. G. Kogan et al., Phys. Rev. B 42, 2631 (1990); A. I. Buzdin and A. Yu. Simonov, Pis'ma Zh. Eksp. Teor. Fiz. 51, 168 (1990) [JETP Lett. 51, 191 (1990)]; A. V. Balatskii et al., Zh. Eksp. Teor. Fiz. 90, 1478 (1986) [Sov. Phys. JETP 63, 866 (1986)]; A. M. Grishin et al., Zh. Eksp. Teor. Fiz. 97, 1930 (1990) [Sov. Phys. JETP 70, 1089 (1990)].

[5] L. Daemon and L. J. Campbell (to be published).

[6] J. P. Rice and D. M. Ginsberg, J. Cryst. Growth 109, 432 (1991).

[7] C. A. Murray et al., Phys. Rev. Lett. 64, 2312 (1990); D. G. Grier et al., Phys. Rev. Lett. 66, 2270 (1991).

[8] G. J. Dolan et al., Phys. Rev. Lett. 62, 827 (1989); L. Ya. Vinnokov et al., in High Temperature Superconductivity from Russia, edited by A. I. Larkin and N. V. Zavaritsky (World Scientific, London, 1989).

[9] A general discussion of flux imaging techniques can be found in R. P. Huebner, Magnetic Flux Structures in Superconductors (Springer-Verlag, New York, 1979).

[10] L. J. Campbell et al., Phys. Rev. B 38, 2439 (1988).

[11] We have taken $\lambda_a = 0.14$ μm, $\lambda_b = 1.15\lambda_a$, and $\lambda_c = 7\lambda_a$.

[12] For the various forms used for the temperature-dependent penetration depth, see M. Tinkham, Introduction to Superconductivity (Krieger, Malabar, 1980).

[13] D. E. Farrell et al., Phys. Rev. Lett. 64, 1573 (1990). The extent of the reversible range is even larger on samples cut from the center of individual crystals, due to increased oxygen homogeneity [D. E. Farrell (private communication)].

[14] J. F. Annett et al., in Physical Properties of High Temperature Superconductors II, edited by D. M. Ginsberg (World Scientific, Singapore, 1990).

[15] D. A. Huse (unpublished). A similar result was found by L. Daemon and L. J. Campbell (private communication).

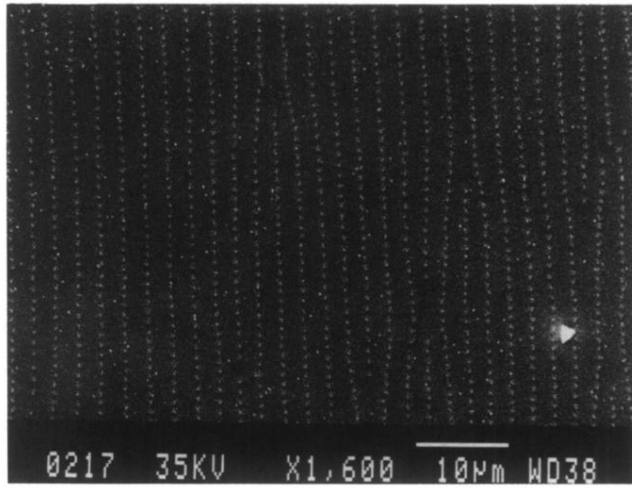[16] A. Sudbo and E. H. Brandt, Phys. Rev. Lett. 67, 3176 (1991).

FIG. 1. SEM micrograph of the vortex chains with a field of 24.8 G applied at 70° from the ĉ axis of the crystal. The chains lie in the plane defined by **B** and ĉ. The resultant image is independent of the direction of the â axis, which in this picture runs approximately 45° from the chains.